JOURNAL OF SPACECRAFT AND ROCKETS
Vol. 35, No. 3, May–June 1998

Launch Vehicle Self-Sustained Oscillation from Aeroelastic Coupling Part 1: Theory

K. W. Dotson,* R. L. Baker,† and B. H. Sako‡
The Aerospace Corporation, Los Angeles, California 90009-2957

Self-sustained oscillation of launch vehicles can result during transonic flight if structural responses couple with alternating flow separation forces at the payload fairing cone–cylinder junction. A new technique for the prediction of the amplitudes of limit cycles induced by this aeroelastic coupling is presented. As in the classical approach, aeroelastic theory is used with semiempirical definition of the forces. Emphasis is placed on establishing the steady-state dynamic behavior of the launch vehicle. A notable feature of the theory is the derivation of simple analytic expressions for the dynamic amplification factor consistent with coupled aeroelastic forces and launch vehicle responses. These equations can be readily evaluated for given structural and flowfield parameters and were validated numerically. The theory also shows that the response of structurally damped launch vehicles undergoing aeroelastic coupling is always bounded.

Nomenclature

$[C^*]$ = system modal damping matrix, lbf-s/in. and lbf-s/rad
C_p = static pressure coefficient, dimensionless
F = maximum value of force resultant, lbf
$F(q)$ = alternating flow force, lbf
$\{F(t)\}$ = vector of system external forces, lbf
g = component of function ξ, dimensionless
$[I]$ = system modal mass matrix (identity matrix), lbm
M = Mach number, dimensionless
n = index in Fourier series, dimensionless
p = static pressure, lbf/in.^{2}
$q(t)$ = generalized translation for a single system mode, in.
$\dot{q}(t)$ = generalized translational velocity for a single system mode, in./s
$\ddot{q}(t)$ = generalized translational acceleration for a single system mode, in./s^2
$\{q(t)\}$ = vector of system generalized translations and rotations, in. and rad
$\{\dot{q}(t)\}$ = vector of system generalized translational and rotational velocities, in./s and rad/s
$\{\ddot{q}(t)\}$ = vector of system generalized translational and rotational accelerations, in./s^2 and rad/s^2
T = period, s
t = time (transient motion), s
u = component of function ξ, dimensionless
W = effective width of payload fairing (PLF) over which flow state alternates, in.
x = distance aft of the PLF cone–cylinder junction, in.
z = generalized translation normalized with respect to its static value, dimensionless
γ = ratio of specific heats, dimensionless
ΔE = normalized energy loss, lbf-in./in.^{2}
Δt = time required for flow state change, s
ΔW = normalized work gain, lbf-in./in.^{2}
δ = displacement parameter, dimensionless
ζ = structural damping (as a ratio to the critical value) for a single system mode, dimensionless
η = aerodynamic stiffness for a single mode, rad^2/s^2
$\dot{\eta}$ = aerodynamic damping for a single mode, rad/s
θ = bending rotation, rad
ξ = force variation, dimensionless
τ = time (steady-state motion), s
ϕ = modal value for a single system mode, 1/lbm
$[\phi]$ = system modes matrix, dimensionless
ψ = phase difference, deg
ω = undamped circular natural frequency of a single system mode, rad/s
$\bar{\omega}$ = damped circular natural frequency of a single system mode, rad/s
$[\omega^2]$ = system modal stiffness matrix, lbf/in. and lbf/rad

Subscripts

a–d = time points in idealized force representation
af = attached flow
cr = critical
e = excitation, also time point in idealized force representation
f = final, also physical force application points
fv = free vibration
i = bending mode number
max = maximum
n = PLF nose
p = pulse
r = rotation
sf = separated flow
sh = shock
st = static
1 = first force resultant
2 = second force resultant
∞ = freestream state

Introduction

TWO flow states may exist on a launch vehicle payload fairing (PLF) during transonic flight. As shown in Fig. 1, the flow at the cone–cylinder junction (CCJ) may be separated or attached. Wind-tunnel test data reported in 1963 demonstrated that, for a given cone–cylinder angle, these flow states can alternate randomly in narrow regions of Mach number and angle of attack.[1,2] Although it has long been acknowledged that the probability of encountering many flow alternations during transonic flight is small,[3] it is possible that the changes in the flow state could tune with the motion of a launch vehicle. No failures or adverse load conditions have been documented for alternating flow separation at the PLF CCJ, but the loss of the Atlas mission with the Able IV spacecraft in the early

Received March 2, 1997; revision received Jan. 28, 1998; accepted for publication Feb. 2, 1998.

*Engineering Specialist, Structural Dynamics Department, P.O. Box 92957-M4/909. Senior Member AIAA.
†Senior Engineering Specialist, Fluid Mechanics Department, P.O. Box 92957-M4/967.
‡Senior Engineering Specialist, Software Support Office, P.O. Box 92957-M4/915.

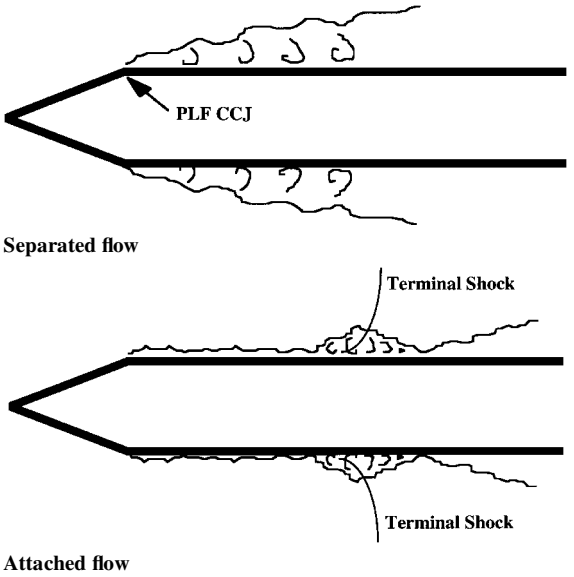

Fig. 1 Flow states at PLF CCJ during transonic flight.

1960s was attributed to aeroelastic coupling caused, analogously, by flow separation at the PLF boat tail.[4]

In 1967 an aeroelastic theory was developed for assessment of theoretical coupling of alternating flow separation forces with structural bending modes.[5] This classical approach is semiempirical in the sense that wind-tunnel test data were used to define the magnitudes of the alternating flow separation forces, and the force variation itself was idealized. More recently, an approach was developed that employs a dynamic representation of the structure coupled with computational fluid dynamics (CFD) to define the nonlinear unsteady aerodynamic pressures.[6] Provided that the flow solver code accurately models the complex transonic regime,[7] this technique is more rigorous than the classical theory, but at the cost of being computationally intensive.

A new aeroelastic technique is presented in this work. The initial assumptions are identical to those that were introduced in Ref. 5 and have been used historically in implementation of the classical theory.[8] The development differs, however, in the treatment of the alternating flow separation forces in the equations of motion. An assessment of self-sustained oscillations induced by aeroelastic coupling is conducted that concludes with the direct prediction of the steady-state amplitude rather than a prima facie limiting value defined ostensibly by stability considerations.[8]

Transonic Airloads Predictions

Airloads Analysis Methodology

The modal equations of motion for the system during transonic flight are defined by

$$[I]\{\ddot{q}(t)\} + [C^*]\{\dot{q}(t)\} + [\omega^2]\{q(t)\} = [\phi]_f^T\{F(t)\} \qquad (1)$$

The vector $\{F(t)\}$ theoretically accounts for all of the external forces. In practice, however, Eq. (1) is broken up into constituent airloads events, which are analyzed separately and are treated statistically.[9] The dynamic components of the airloads consist of those induced by buffeting, gust, control system parameters, and maneuvering.[9] Mean and dispersed values for each of the dynamic components are predicted, and total loads are computed on the day of launch using a loads combination equation.[10] Along with the liftoff event, maximum airloading induces the most important loads for the design of an expendable launch vehicle.[9] As an airloads event, aeroelastic coupling can therefore increase the total launch vehicle loads that the structure must withstand.

Aeroelastic Coupling Analysis Limitations

The launch vehicle control system reacts to the vehicle motion induced by external forces and steers it to maintain a trim condition.[11] Because the control forces lag in time the aeroelastic forces,[11] a thorough treatment of the aeroelastic coupling phenomenon should include an active control system. Neither the classical theory nor the CFD approach models the launch vehicle control system or even acknowledges this interaction.[5,6]

The importance of other transonic events on aeroelastic coupling has also not been assessed. An analysis including flight winds may reveal that launch vehicle maneuvers hinder the development of self-sustained oscillations from aeroelastic coupling. For instance, an analogous study conducted for the Titan IV launch vehicle showed that limit cycles induced by control system parameters cannot develop during launch vehicle steering.[12]

A comprehensive treatment of this complex phenomenon is beyond the state of the art. The objective of the present theory is to provide a phenomenological model from which key parameters may be identified and estimates of launch vehicle responses and loads can be readily obtained. It is believed that the complications mentioned earlier cannot be assessed without first developing a thorough understanding of the fundamental force–response relationship that characterizes launch vehicle aeroelastic coupling. Extension of the theory to include control-structure interaction and the effects of other transonic events is an important topic for future study.

Aeroelastic Theory

Aerodynamic Flowfield Definition

The current problem is driven by forces on the PLF that undergo essentially step changes in magnitude each time the flow alternates from attached to separated or vice versa at the CCJ. A thorough development of the time histories of these forces and a description of the coupling to the vehicle response are given later. The information needed to define the forces acting on the PLF is given by the longitudinal profiles of the pressure coefficient for the separated and attached flow states. The pressure coefficient C_p and the local static pressure p are related by

$$C_p = 2\frac{p - p_\infty}{\gamma M_\infty^2 p_\infty} \qquad (2)$$

Curves of the pressure coefficient corresponding to separated and attached flows for the Titan IV launch vehicle are shown in Fig. 2 for a zero angle of attack and a freestream Mach number of 0.8. The pressure profiles change somewhat as a function of the freestream Mach number, and aeroelastic coupling is generally evaluated in the classical theory for more than one time point in the transonic regime.

The profile for attached flow $C_{p,\mathrm{af}}$ was obtained from wind-tunnel test data for the Titan vehicle.[13] The profile for separated flow $C_{p,\mathrm{sf}}$ was obtained from Ref. 2; the separated flow condition was not observed in the Titan wind-tunnel tests. The $C_{p,\mathrm{sf}}$ data plotted correspond to a 20-deg cone angle, which represents the average of the two angles (25 and 15 deg) for the Titan IV PLF biconic forecone. The average angle for a biconic configuration was also selected in Ref. 5 in the analysis of the Saturn booster. Static pressure measurements obtained from flight data for the Titan IV indicate reasonably good agreement with both the separated flow and the attached flow wind-tunnel data in Fig. 2.

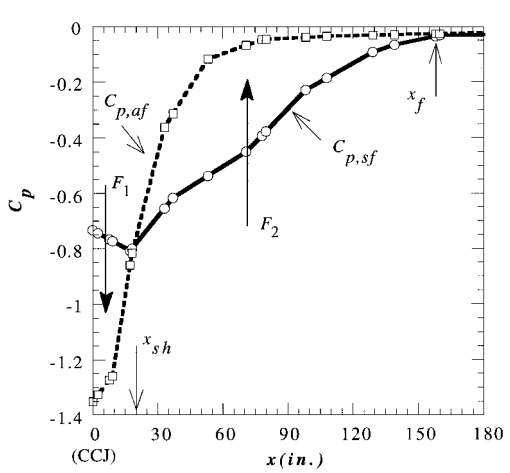

Fig. 2 Pressure coefficient profiles for Titan IV with a zero angle of attack and a freestream Mach number of 0.8.

In the implementation of the classical theory,[8] the continuous force corresponding to the change from attached to separated flow at the CCJ is expressed as two resultants, as shown in Fig. 2. Two forces obviously provide a better discrete representation for analysis than a single resultant, but the decomposition of the continuous force into exactly two components is arbitrary. Using Eq. (2), these forces and their locations on the PLF are defined by

$$F_1 = \frac{\gamma}{2} M_\infty^2 p_\infty W \int_0^{x_{sh}} (C_{p,sf} - C_{p,af})\,dx \tag{3}$$

$$F_2 = \frac{\gamma}{2} M_\infty^2 p_\infty W \int_{x_{sh}}^{x_f} (C_{p,af} - C_{p,sf})\,dx \tag{4}$$

$$x_1 = \frac{\int_0^{x_{sh}} (C_{p,sf} - C_{p,af}) x\,dx}{\int_0^{x_{sh}} (C_{p,sf} - C_{p,af})\,dx} \tag{5}$$

$$x_2 = \frac{\int_{x_{sh}}^{x_f} (C_{p,af} - C_{p,sf}) x\,dx}{\int_{x_{sh}}^{x_f} (C_{p,af} - C_{p,sf})\,dx} \tag{6}$$

The length x_{sh} defines the distance from the CCJ to the terminal shock location for the attached flow. For purposes of calculating the resultants, the location of x_{sh} is taken as the point where the $C_{p,af}$ and the $C_{p,sf}$ profiles cross one another. The forces F_1 and F_2 equal 1500 and 5900 lbf, respectively, for the curves shown in Fig. 2 and the Titan IV aerodynamic parameters.

Aeroelastic Coupling Formulations

The two force resultants are assumed in the implementation of the classical theory to couple with vehicle motion in a single bending mode.[8] The single mode representation is then used to analyze aeroelastic coupling for each of the lower bending modes independently. Extracting from the full set the modal equation that best represents the ith system bending mode yields

$$\ddot{q}_i(t) + 2\zeta_i \omega_i \dot{q}_i(t) + \omega_i^2 q_i(t) = \phi_{i,1} F_1(q_i) + \phi_{i,2} F_2(q_i) \tag{7}$$

in which the modal values $\phi_{i,1}$ and $\phi_{i,2}$ correspond to translational degrees of freedom (DOFs) in the plane of the force application.

In the classical theory, Eq. (7) is effectively rewritten as

$$\ddot{q}_i(t) + (2\zeta_i \omega_i + \dot{\eta}_i)\dot{q}_i(t) + \left(\omega_i^2 + \eta_i\right) q_i(t) = 0 \tag{8}$$

in which the two force resultants have been converted into aerodynamic stiffness and damping terms. Depending on the magnitudes and signs of the force resultants, the aerodynamic damping term can be positive or negative. So-called undamping corresponds to negative values of $\dot{\eta}_i$. The classical theory assumes that arbitrary values of undamping may exist such that the total damping (represented by the sum preceding the generalized velocity) may be greater or less than zero. A so-called stability criterion is then established by setting the total damping equal to zero.[8] The result is a limit cycle amplitude perceived to represent the threshold at which the system response becomes unbounded. However, it is shown herein that the semiempirical force definition always yields a bounded limit cycle, such that a stability criterion for divergence does not exist. This conclusion is reached by leaving the generalized forces on the right-hand side of Eq. (7) and by finding a solution based on the definition of the coupled force and response.

Self-Sustained Oscillations

Equation for Periodic Motion

The two force resultants are merely a discrete representation of the continuous force at the PLF CCJ during the changes in flow state and have the same variation in time. Equation (7) can, therefore, be expressed as

$$\ddot{q}(t) + 2\zeta\omega\dot{q}(t) + \omega^2 q(t) = (\phi_1 F_1 + \phi_2 F_2)\boldsymbol{\xi}(q) \tag{9}$$

in which the subscript i has been dropped for convenience. The special case in which the response has converged after transient aeroelastic coupling to a limit cycle is considered next. In this condition, the launch vehicle oscillations are self-sustaining; that is, they repeat unless the forces cease. Because of the periodicity, it is necessary to consider only one cycle of the coupled force and response, and Eq. (9) can be written as

$$\ddot{q}(\tau) + 2\zeta\omega\dot{q}(\tau) + \omega^2 q(\tau) = (\phi_1 F_1 + \phi_2 F_2)\boldsymbol{\xi}(q) \qquad 0 \le \tau \le T_e \tag{10}$$

The maximum static value of the generalized response is defined by

$$q_{st} = \omega^{-2} |\phi_1 F_1 + \phi_2 F_2| \tag{11}$$

Normalizing Eq. (10) with respect to this value yields

$$\ddot{z}(\tau) + 2\zeta\omega\dot{z}(\tau) + \omega^2 z(\tau) = \omega^2 \boldsymbol{\xi}(z), \qquad 0 \le \tau \le T_e \tag{12}$$

The dynamic amplification factor (AF) for the steady-state motion is simply given by

$$\mathrm{AF} = |z_{max}| \tag{13}$$

Finally, the limit cycle amplitude, expressed as the bending rotation at the tip of the PLF nose, is defined as

$$\theta_{max} = \mathrm{AF} |\phi_{r,n}| q_{st} \tag{14}$$

If Eq. (13) does not admit a solution, the system is not periodic and either tends to rest or becomes unbounded. It is shown herein that the latter does not occur.

Force Variation for Aeroelastic Coupling

A schematic of one cycle of the idealized coupled force and response is shown in Fig. 3. It is assumed that the forcing function is dominated by the flow state, i.e., whether the flow is separated or attached. It is further assumed that the rate of deflection is sufficiently slow such that the flow is quasisteady except during the transition between flow states. Changes in the flow state occur when the deflection angle equals a critical value.

Referring to Fig. 3, the coupling can be described as follows:

1) The deflection of the PLF nose reaches the critical angle, ($\tau = t_a$).

2) The flow state changes during a time interval Δt, ($t_a \le \tau \le t_b$).

3) The flow remains in the new state until the PLF nose returns to the critical value, ($t_b < \tau < t_c$).

4) The flow reverts to its nominal state after a time interval Δt, ($t_c \le \tau \le t_d$).

5) The flow remains in the nominal state while the PLF continues to deflect, ($t_d < \tau < t_e$).

6) The deflection of the PLF nose reaches the critical angle in the opposite direction, ($\tau = t_e$).

7) The process continues.

In Fig. 3, the response oscillates about zero, and flow state changes occur on both sides of the PLF. In principle, the launch vehicle

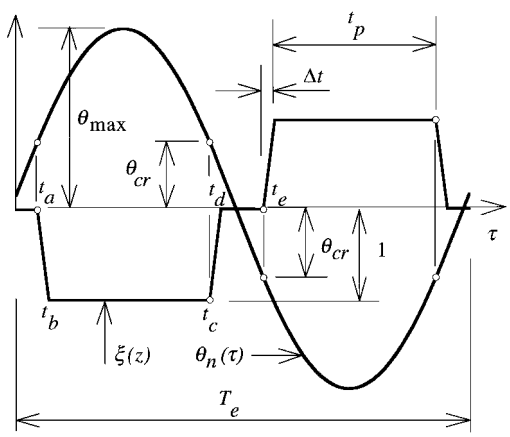

Fig. 3 Schematic of one cycle of steady-state coupled force and response.

can also experience a quasisteady angle of attack during aeroelastic coupling such that the changes in flow state occur only on one side of the PLF. However, launch vehicles generally use a steering program that minimizes the angle of attack and have an onboard control system that maneuvers the vehicle into the sensed wind.[9,11] As a result, the angle of attack is, in practice, generally quite small. For this reason, two-sided flow state changes are addressed in this work. Note, however, that PLF nose cone angles less than 20 deg or greater than 25 deg may preclude flow alternations at or near zero angle of attack.[5] For launch vehicles in these categories, one-sided changes occurring at a quasisteady angle of attack represent the only possible scenario for aeroelastic coupling. The approach described herein can also be extended to this less common problem.

Steady-State Amplification Factor

In this section analytic expressions for AF are derived assuming the function $\xi(z)$ has a linear variation during the time lag Δt. These equations were validated numerically, and comparisons of the results are provided. It is also proved that the response and force must be out of phase, as shown in Fig. 3, for aeroelastic coupling to occur. The analytic expressions and the numerical simulation demonstrate that the ratio of the period of the excitation to that of the bending mode, T_e/T_i, must be less than unity for this condition to prevail. All of the equations for the dynamic amplification factor that follow correspond to $T_e/T_i < 1$.

Procedure

Equation (12) is weakly nonlinear because the force term on the right-hand side is a function of the displacement z and is not known a priori as a function of time. A trial function for the nonlinear response is defined herein as a slightly shifted version of the undamped linear solution for a single-DOF (SDOF) system subjected to the force variation. The excitation period is treated as an adjustable parameter defined by energy principles once the trial function has been established. The approach is fundamentally similar to techniques such as collocation, Galerkin's method, and the method of least squares.[14]

The trial function is defined by formally solving the differential equation over the piecewise linear segments of the force variation and by satisfying the appropriate periodicity condition. This technique for obtaining closed-form expressions for the periodic response of SDOF systems subjected to nonharmonic forces was developed in Ref. 15. Inspection of Fig. 3 reveals that there are 9 piecewise linear segments over the excitation period and, consequently, 18 unknown constants in the linear solution. (The antisymmetry of the force variation could be used to reduce to 10 the number of unknowns.[15]) Continuity of displacement and velocity at the segment interfaces defines 16 of these constants. The remaining two conditions come from the periodicity requirement, namely, that the response must be identical at the beginning and end of the excitation period.

The undamped solution is used because bending modes typically have $\zeta < 3\%$, and such low values of structural damping have a negligible effect on the amplitude and phase of the steady-state response of systems with $T_e/T_i < 1$ (Ref. 15). For instance, Fig. 4 shows the amplification factor for $t_p = T_e/2$ and $T_e \gg \Delta t$, referred to herein as alternating step excitation. The undamped solution is in excellent agreement with the damped response for all values of T_e/T_i not very close to resonance. It will be shown that, although structural damping does not significantly affect the shape and phase of the trial function, it is a critical parameter in the definition of the excitation period.

The undamped response is antisymmetric (with zero crossings at $\tau = 0, T_e/2$, and T_e) and does not satisfy the requirement that the bending rotation equal the critical value at each of the time points shown as circles in Fig. 3. Simply shifting the linear solution in the direction of the origin by the amount $\Delta t/2$ makes it admissible as a trial function for the nonlinear system. The phase difference (in degrees) between the force and response is, therefore, given by

$$\psi = 180(1 - \Delta t/T_e) \tag{15}$$

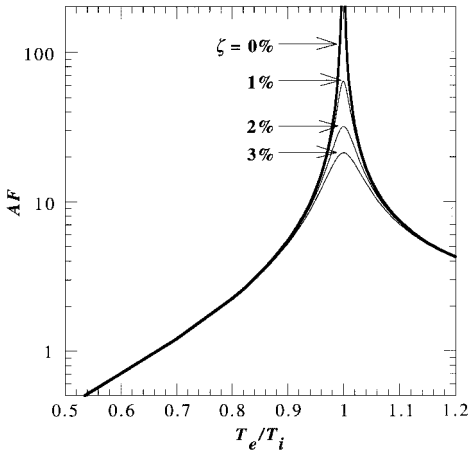

Fig. 4 Effects of damping on steady-state amplification factor for alternating step excitation.

Analytic Expressions

The trial function has one maximum (or minimum) at the midpoint of each half-cycle. The displacement at these time points yields the following analytic expression for the dynamic amplification factor:

$$\mathrm{AF} = \frac{[\sin(\omega\Delta t)/\omega\Delta t]\cos(\omega t_a) - \{[1 - \cos(\omega\Delta t)]/\omega\Delta t\}\sin(\omega t_a)}{\cos(\omega T_e/4)} - 1 \tag{16}$$

Equation (16) is valid for all nonnegative values of t_p, t_a, and Δt that satisfy the relationship

$$T_e/2 = t_p + 2t_a + 2\Delta t \tag{17}$$

For aeroelastic coupling, the period of the excitation is on the order of the period of the bending mode, whereas Δt reflects the time for flow changes and is much smaller in duration. The analytic expression for the amplification factor can, therefore, generally be approximated by

$$\mathrm{AF} = \frac{\cos(\omega t_a)}{\cos(\omega T_e/4)} - 1 \tag{18}$$

The result of Eq. (18) is greater than that of Eq. (16). The time point t_a is a measure of the dead zone in the force variation. Rewriting Eq. (18) in terms of the force pulse width yields

$$\mathrm{AF} = \frac{\cos[\omega(T_e/4 - t_p/2)]}{\cos(\omega T_e/4)} - 1 \tag{19}$$

The maximum value of AF corresponds to alternating step excitation and is given by

$$\mathrm{AF} = \sec(\omega T_e/4) - 1 \tag{20}$$

Effect of Critical Rotation

The normalized bending displacement consistent with the critical PLF nose rotation is defined by

$$z_{\mathrm{cr}} = \frac{\theta_{\mathrm{cr}}}{|\phi_{r,n}|\, q_{\mathrm{st}}} \tag{21}$$

The constraint that the trial function equals z_{cr} at the initiation points for the force changes yields

$$(2z_{\mathrm{cr}} + 1)\cos(\omega T_e/4) = (\omega\Delta t)\sin(\omega T_e/4 - 2\omega t_a) + \cos(\omega T_e/4 - 2\omega t_a) + 0(\Delta t^2) \tag{22}$$

Equation (22) shows that the dead zone in the force variation disappears, i.e., $t_a = 0$, when

$$z_{\mathrm{cr}} = (\omega\Delta t/2)\tan(\omega T_e/4) \tag{23}$$

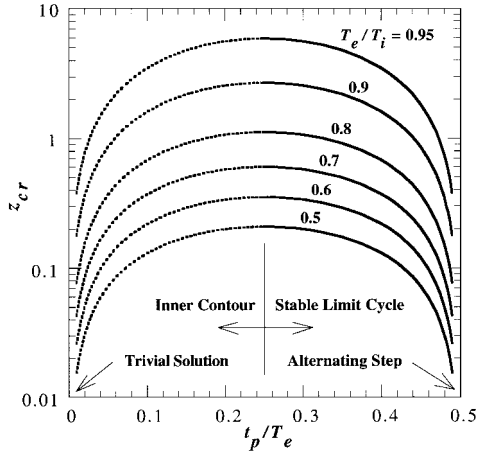

Fig. 5 Admissible force pulse widths for stable limit cycle.

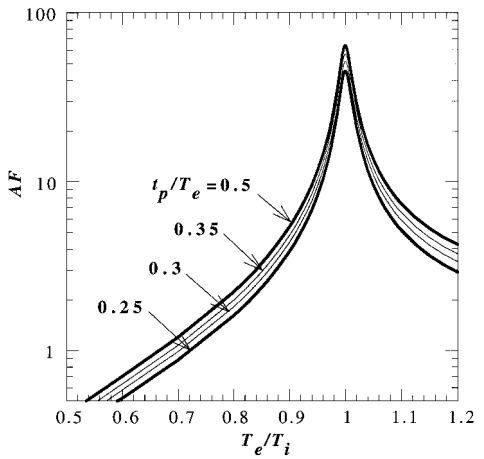

Fig. 6 Effect of pulse width on steady-state amplification factor (ζ = 1%).

For $T_e \gg \Delta t$, Eq. (22) yields the force pulse widths

$$t_p/T_e = \tfrac{1}{4} \pm (1/\omega T_e)\cos^{-1}[(2z_{\rm cr}+1)\cos(\omega T_e/4)] \tag{24}$$

Equation (24) is illustrated in Fig. 5. Two unique force pulse widths exist for any combination of T_e/T_i and $z_{\rm cr}$. The larger of these values defines the force variation for the stable limit cycle, whereas the smaller corresponds to the threshold at which responses tend either to rest or to the stable limit cycle. Figure 5 also shows that there is a value of $z_{\rm cr}$ above which the analytic expression does not admit a solution for a specified value of T_e/T_i; if the forces are too small or if the critical nose angle for alternating flow is too large, the system tends to rest rather than to a limit cycle. Using Eq. (24), it can be shown that self-sustained oscillations exist only for

$$z_{\rm cr} \le \frac{\sec(\omega T_e/4) - 1}{2} \tag{25}$$

The effect of the force pulse width on the amplification factor for stable limit cycles is shown in Fig. 6. The data used to construct these curves were defined numerically, and damping was assumed to equal 1%. The width of the force pulse, and hence the value of $z_{\rm cr}$, does not have a dramatic effect on the amplification factor. The plotted data for the damped response are in excellent agreement with Eq. (19) for values of T_e/T_i not very close to the resonant peak; the differences increase to 5% at $T_e/T_i = 0.97$. This further validates the use of an undamped trial function if the period of the excitation is not extremely close to that of the bending mode.

Free-Vibration Amplification Factor

The time during which the launch vehicle flies through the transonic region is, of course, of finite duration. The flow at the PLF CCJ, therefore, ultimately ceases to alternate, and in the absence of other external forces, the launch vehicle undergoes free vibration. By definition, the alternations may cease in one of only two states: with the force present and constant or at a half or full cycle with zero force. In the former, the free vibration is bounded by the limit cycle amplitude, but in the latter the first maximum during free vibration exceeds the steady-state response. A derivation of the corresponding amplification factor follows.

At the end of a half or full cycle of excitation, the displacement equals zero. Using the velocity at this time point as an initial condition yields the following expression for the damped free-vibration response:

$$z(t) = \pm\left\{\left[\frac{\sin(\omega\Delta t)}{\omega\Delta t}\right]\left[\tan\left(\frac{\omega T_e}{4}\right)\cos(\omega t_a) - \sin(\omega t_a)\right] - \left[\frac{1-\cos(\omega\Delta t)}{\omega\Delta t}\right]\left[\tan\left(\frac{\omega T_e}{4}\right)\sin(\omega t_a) + \cos(\omega t_a)\right]\right\} \times e^{-\zeta\omega t}\left[\frac{\omega\sin(\bar{\omega}t)}{\bar{\omega}}\right] \tag{26}$$

in which the origin of time t coincides with free vibration. The largest response, of course, occurs in the first half-cycle of free vibration, and ignoring higher-order damping terms, the dynamic amplification factor is defined by

$$\mathrm{AF_{fv}} = \left\{\left[\frac{\sin(\omega\Delta t)}{\omega\Delta t}\right]\left[\tan\left(\frac{\omega T_e}{4}\right)\cos(\omega t_a) - \sin(\omega t_a)\right] - \left[\frac{1-\cos(\omega\Delta t)}{\omega\Delta t}\right]\left[\tan\left(\frac{\omega T_e}{4}\right)\sin(\omega t_a) + \cos(\omega t_a)\right]\right\} \times \exp\left(-\frac{\pi\zeta}{2\sqrt{1-\zeta^2}}\right) \tag{27}$$

Equation (27) can generally be approximated by

$$\mathrm{AF_{fv}} = \left[\tan\left(\frac{\omega T_e}{4}\right)\cos(\omega t_a) - \sin(\omega t_a)\right]\exp\left(-\frac{\pi\zeta}{2\sqrt{1-\zeta^2}}\right) \tag{28}$$

Rewriting Eq. (28) as an explicit function of the force pulse width yields

$$\mathrm{AF_{fv}} = \left\{\tan\left(\frac{\omega T_e}{4}\right)\cos\left[\omega\left(\frac{T_e}{4} - \frac{t_p}{2}\right)\right] - \sin\left[\omega\left(\frac{T_e}{4} - \frac{t_p}{2}\right)\right]\right\}\exp\left(-\frac{\pi\zeta}{2\sqrt{1-\zeta^2}}\right) \tag{29}$$

The maximum amplification factor for free vibration corresponds to alternating step forced excitation and is given by

$$\mathrm{AF_{fv}} = \tan\left(\frac{\omega T_e}{4}\right)\exp\left(-\frac{\pi\zeta}{2\sqrt{1-\zeta^2}}\right) \tag{30}$$

Using Eqs. (19) and (29), one can show that

$$\frac{\mathrm{AF_{fv}}}{\mathrm{AF}} = \left\{\frac{\cos(\omega t_p/4)}{\sin[\omega(T_e/4 - t_p/4)]}\right\}\exp\left(-\frac{\pi\zeta}{2\sqrt{1-\zeta^2}}\right) \tag{31}$$

The first bracketed term is plotted in Fig. 7. The difference between the steady-state and free-vibration amplification factors is greatest when T_e/T_i is not large and diminishes as resonance is approached.

The adjustable parameter T_e must be defined before the analytic expressions can be evaluated. This derivation and numerical investigations of aeroelastic coupling are provided in the next section.

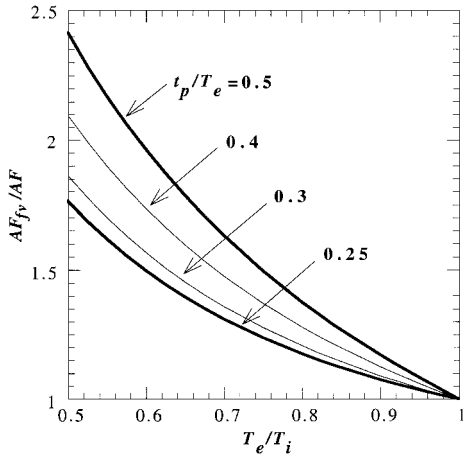

Fig. 7 Effect of free vibration on amplification factor.

Numerical Simulation

Procedure

The analytic expressions correspond to steady-state motion and a linear force variation during the time lag Δt. The numerical analysis, in contrast, includes the transient phase of the response and defines the ramp as a quarter-cycle of a squared sinusoid in the displacement domain. The latter feature is introduced to eliminate discontinuities at the endpoints of the function that could compromise the stability of the numerical analysis. When the time lag is small with respect to the period of the excitation, the squared sinusoid yields a force variation in the time domain that is, for all practical purposes, linear during the lag. The force variation, therefore, strongly resembles that shown in Fig. 3. It is initially assumed that the force is out of phase with the response; however, the importance of this phasing is investigated.

Figure 8 shows a schematic of the phase plane diagram for one response cycle. The top and bottom parts illustrate the force variation defined by

$$\xi = u(z) + g(z, \operatorname{sgn} \dot{z}) \tag{32}$$

in which

$$u(z) = 1, \qquad -z - z_{cr} > \delta \tag{33a}$$

$$u(z) = 0, \qquad -z_{cr} < z < z_{cr} \tag{33b}$$

$$u(z) = -1, \qquad z - z_{cr} > \delta \tag{33c}$$

$$u(z) = \sin^2\left[\frac{\pi(z + z_{cr})}{2\delta}\right], \qquad 0 \le -z - z_{cr} \le \delta \tag{33d}$$

$$u(z) = -\sin^2\left[\frac{\pi(z - z_{cr})}{2\delta}\right], \qquad 0 \le z - z_{cr} \le \delta \tag{33e}$$

$$g(z, \operatorname{sgn} \dot{z}) = \cos^2\left[\frac{\pi(z + z_{cr})}{2\delta}\right]$$

$$-\delta \le -z - z_{cr} \le \delta, \qquad \dot{z} > 0 \tag{34a}$$

$$g(z, \operatorname{sgn} \dot{z}) = -\cos^2\left[\frac{\pi(z - z_{cr})}{2\delta}\right]$$

$$-\delta \le z - z_{cr} \le \delta, \qquad \dot{z} < 0 \tag{34b}$$

$$g(z, \operatorname{sgn} \dot{z}) = 0 \qquad \text{for all other values of } z \tag{34c}$$

and $0 < \delta \le z_{cr}$. A computer program of the Duhamel integral method for piecewise linear forces[16] was used to evaluate Eq. (12), which is now valid for all time, given initial values of displacement and velocity. Convergence of the solution was verified by reducing the integration time step. The value of δ was chosen such that the steady-state force variation exhibited the desired time lag Δt.

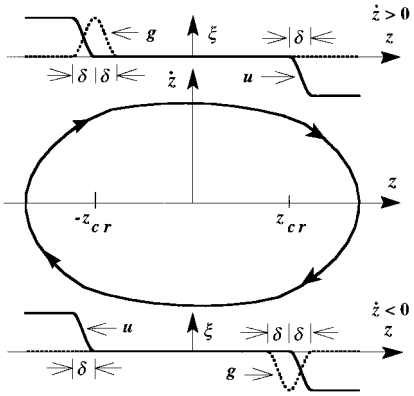

Fig. 8 Schematic of force variation and phase plane diagram for stable limit cycle.

Energy Relationships

In the absence of the function g, structural damping causes the system to spiral to a state of rest in the phase plane. Systems undergoing aeroelastic coupling attain a limit cycle because the work conducted by the function g offsets the energy loss due to damping. In one cycle, the latter is defined by

$$\Delta E = \int_{z(0)}^{z(T_e)} 2\zeta\omega\dot{z}\,\mathrm{d}z = 2\zeta\omega\int_0^{T_e} \dot{z}^2\,\mathrm{d}\tau \tag{35}$$

The work conducted by the function g in the top part of Fig. 8 is positive because this force and the change in the response are both positive. Similarly, the function g in the bottom part of Fig. 8 produces positive work because the change in the response is negative during application of this negative force. The total work conducted during one cycle is, therefore, positive and defined by

$$\Delta W = \omega^2\int_{z_{cr}-\delta}^{z_{cr}+\delta} \cos^2\left[\frac{\pi(z - z_{cr})}{2\delta}\right]\mathrm{d}z + \omega^2\int_{-z_{cr}-\delta}^{-z_{cr}+\delta} \cos^2\left[\frac{\pi(z + z_{cr})}{2\delta}\right]\mathrm{d}z = 2\omega^2\delta \tag{36}$$

Equating the energy loss over one cycle with the work gain yields

$$\int_0^{T_e} \dot{z}^2\,\mathrm{d}\tau = \frac{\omega\delta}{\zeta} \tag{37}$$

The numerical simulation verifies exactly the preceding identity for the limit cycle state. For $T_e \gg \Delta t$, the displacement parameter can be approximated by

$$\delta = \dot{z}_{cr}\Delta t \tag{38}$$

Substituting Eq. (38) into Eq. (37) yields

$$\int_0^{T_e} \dot{z}^2\,\mathrm{d}\tau = \dot{z}_{cr}\left(\frac{\omega\Delta t}{\zeta}\right) \tag{39}$$

Excitation Period

Equation (39) was evaluated using the trial function. The following characteristic equation is the result for $z_{cr} = 0$:

$$(T_e/T_i)\csc(\omega T_e/2) - 1/\pi = \Delta t/\zeta T_i \tag{40}$$

The relationship for nonzero values of z_{cr} is more complicated but yields values of T_e/T_i that are, for all practical purposes, identical to those from Eq. (40). The excitation period, in other words, is a very weak function of the critical nose angle. The roots T_e/T_i are illustrated in Fig. 9 with respect to the ratio of the known variables $\Delta t/\zeta T_i$. Increasing the time lag or the frequency of the bending mode pushes the system closer to a resonant condition. Decreasing structural damping has the same effect. It can be concluded from

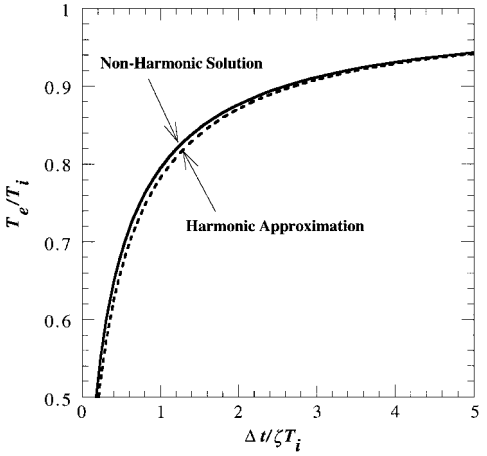

Fig. 9 Normalized period of stable limit cycle.

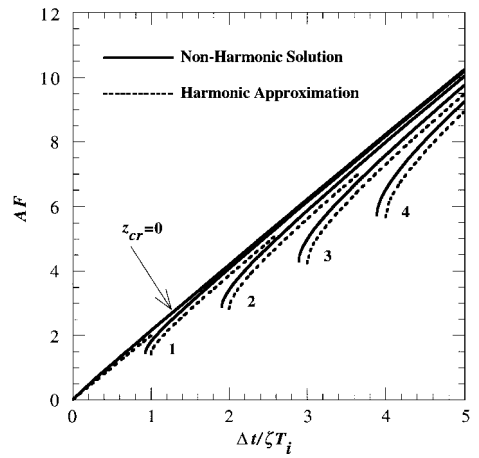

Fig. 10 Amplification factor as a direct function of system variables.

Fig. 9 that the analytic expressions developed in the preceding sections are useful for values of $\Delta t/\zeta T_i$ up to at least 5.

Fourier analysis has traditionally been used to analyze SDOF systems subjected to periodic, nonharmonic excitation.[16] The trial function derived herein is a closed-form expression of the result of Fourier analysis when all of the terms in the series are retained.[15] In some situations, a single term provides a reasonable approximation for the nonharmonic response.[15] In other words, the system may respond as if the force were harmonic with the amplitude of the term selected. Provided $T_e \gg \Delta t$, the Fourier series expansion of the force variation is defined by

$$\xi(\tau) = \left(-\frac{4}{\pi}\right) \sum_{n=1,3,5,\ldots}^{\infty} \left(\frac{1}{n}\right) \sin\left(\frac{n\pi}{2}\right) \sin\left(\frac{n\pi t_p}{T_e}\right) \sin\left(\frac{2n\pi\tau}{T_e}\right) \quad (41)$$

Substituting into Eq. (39) the response of a SDOF system subjected to the first term in this series (with $t_p/T_e = 0.5$) yields

$$T_e/T_i = (1 + 4\zeta/\omega\Delta t)^{-\frac{1}{2}} \quad (42)$$

This harmonic approximation is compared in Fig. 9 with the solution from the nonharmonic trial function. The agreement is reasonable, particularly for the higher values of $\Delta t/\zeta T_i$.

Amplification Factor as Direct Function of System Variables

The roots of Eq. (40) for given values of the salient ratio $\Delta t/\zeta T_i$ were substituted into Eq. (24) to obtain the force pulse widths corresponding to a specified critical deflection z_{cr}. These consistent values of T_e/T_i and t_p/T_e were then substituted into Eq. (19) to obtain the curves plotted in Fig. 10. Note that the amplification factors for nonzero values of z_{cr} are bounded by the curve for zero critical deflection and begin at an initial value of $\Delta t/\zeta T_i$ for self-sustained oscillation. The approximation

$$\mathrm{AF} = 2\left(\frac{\Delta t}{\zeta T_i}\right) \cos\left\{\frac{\sin^{-1}[z_{cr}(\zeta T_i/\Delta t)]}{2}\right\} \quad (43)$$

is also plotted in Fig. 10 and was derived by substituting a harmonic function with flow state changes at z_{cr} into Eq. (39). For zero critical deflection, Eq. (43) reduces to

$$\mathrm{AF} = 2(\Delta t/\zeta T_i) \quad (44)$$

Equation (44) underpredicts the corresponding nonharmonic solution by as much as 15% but concisely illustrates the relative importance of the time lag, structural damping, and period of the bending mode.

It can be concluded from Fig. 10 that the assumed force–response relationship leads to a bounded limit cycle unless the structural damping precisely equals zero, an unrealistic condition. The system response, in other words, cannot diverge. Why then does the classical theory claim that the response may increase with time without limit?[8] The classical theory defines the stability criterion as the amplitude of the limit cycle oscillation for which the total system damping equals zero [see Eq. (8)] and then concludes that for amplitudes smaller than this value the total damping is negative, yielding a divergent system response. But it was shown herein that, given the salient ratio $\Delta t/\zeta T_i$, only one response amplitude is admissible. Arbitrarily decreasing this amplitude to render the total system damping negative is, therefore, inappropriate.

The classical theory uses, without qualification, an undamped harmonic response for the solution of Eq. (8). Indeed, it can be shown that the so-called stability criterion has exactly the form of Eq. (44) when a time lag is explicitly defined.[17] Note, however, that Ref. 5 argues that the launch vehicle response only couples with flow alternations on one side of the PLF and assumes that the force changes instantaneously after the time lag rather than ramps linearly as shown in Fig. 3. It can be shown that the net work done by the classical (one-sided and instantaneous) force variation is identical to that derived for the present (two-sided and ramped) theory if the time lag is numerically equal to the flow transition time Δt. Further comparisons of these two approaches are provided in Ref. 17.

Comparison with Analytic Expressions

A phase plane diagram from a numerical simulation is shown in Fig. 11. For this example, the system frequency and structural

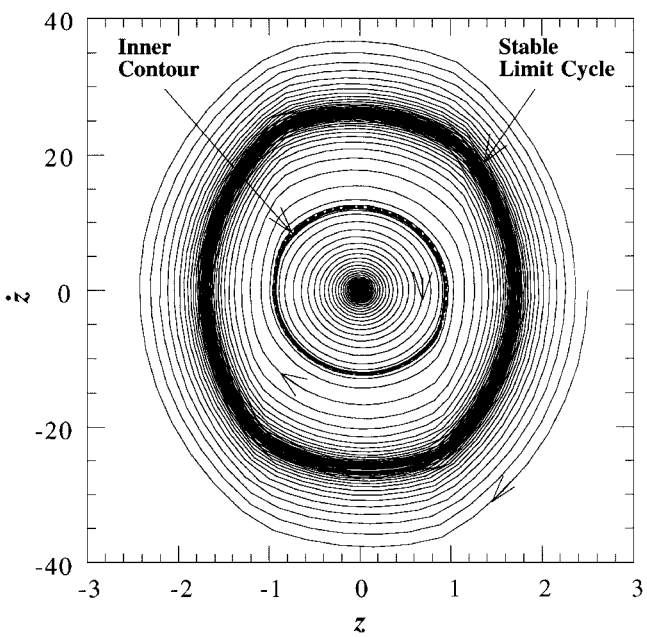

Fig. 11 Numerical simulation phase plane diagram with force and response out of phase (f = 2 Hz, ζ = 2%, z_{cr} = 1, and Δt = 10 ms).

Table 1 Comparison of simulation and analytic results

Property	Simulation result	Analytic expressions		
		Result	Approximation	Eq.
T_e/T_i	0.79	0.79	——	(40)
	——	0.78	Harmonic	(42)
ψ, deg	175	175	——	(15)
t_a/T_e	0.09	0.09	——	(22)
t_p/T_e	0.27	0.27	——	(17)
	——	0.30	$\Delta t/T_e \approx 0$	(24)
AF	1.7	1.7	——	(16)
	——	1.7	$\Delta t/T_e \approx 0$	(19)
	——	2.1	$t_p/T_e \approx 0.5$	(20)
	——	1.4	Harmonic	(43)
AF_{fv}	2.0	2.0	——	(27)
	——	2.0	$\Delta t/T_e \approx 0$	(29)
	——	2.8	$t_p/T_e \approx 0.5$	(30)

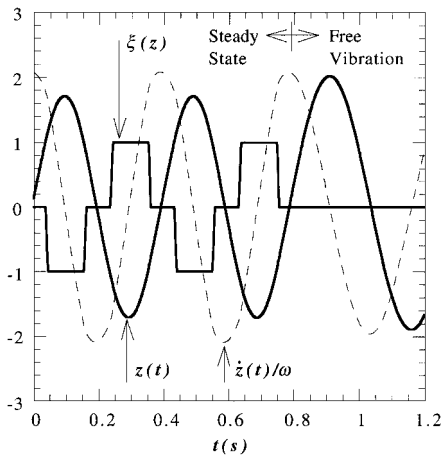

Fig. 12 Numerical simulation time histories with force and response out of phase (f = 2 Hz, ζ = 2%, z_{cr} = 1, and Δt = 10 ms).

damping were taken as 2 Hz and 2%, respectively, and the time lag was assumed to equal 10 ms. The salient ratio $\Delta t/\zeta T_i$, therefore, equaled unity. A unit value of z_{cr} was also assumed. The displacement parameter $\delta = 0.23$ yielded the desired time lag.

The phase plane diagram has a stable singular point, represented by the rest condition, and a stable limit cycle. An inner contour also exists such that initial conditions lying inside its periphery yield responses that tend to rest, whereas those outside yield responses that tend to the stable limit cycle. The force variation at the inner contour differs somewhat from the analytic variation because of the constraints on Eqs. (33) and (34). This polycyclic configuration is common for self-sustained oscillation, and because the initial conditions must exceed a specific value to induce a limit cycle, aeroelastic coupling can be classified as hard self-excitation.[18]

Figure 12 shows time histories corresponding to the limit cycle in Fig. 11. Free vibration was induced by stopping the coupling relationship at the end of a full cycle. Properties of the response are compared in Table 1 with those predicted by the analytic expressions. The simulation phase difference ψ was computed using a cross-correlation function. The comparison attests that the analytic expressions are in agreement with the simulation results and that the ramp in the force variation has a negligible effect on the dynamic amplification factor.

Phasing of Force and Response

The preceding derivation based on energy principles was predicated on the response being out of phase with the force. For the case in which the force and response are in phase, the signs of the functions u and g in Fig. 8 are reversed. The work conducted by the function g during each cycle of the response, therefore, is negative when the force is in phase with the response. Rather than balancing the energy loss due to damping, the flow state changes increase the energy dissipation during each cycle. Figure 13 shows simulation time histories for this scenario with the system inputs from the out-

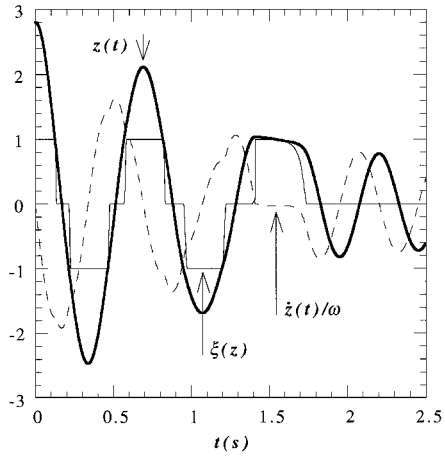

Fig. 13 Numerical simulation time histories with force and response in phase (f = 2 Hz, ζ = 2%, z_{cr} = 1, and Δt = 10 ms).

of-phase example. The response fails to exceed $\pm z_{cr}$ after just two cycles, and the system tends to rest.

It is a longstanding conclusion that the alternating flow separation forces must be out of phase with the launch vehicle response for limit cycles to occur.[19] The present theory has explained the energy transfer caused by the time lag and demonstrated this requirement. The importance of the phasing between the force and response is not unique to aeroelastic coupling and can be generalized for problems in which there is a transfer of energy between a fluid and any oscillating body.[20]

Conclusions

Analytic expressions for the limit cycle state and for the free vibration that occurs when the coupling ceases can be derived without converting the alternating flow separation forces into aeroelastic stiffness and damping terms. Numerical simulations validate the accuracy of these equations. The system response is always finite for the assumed force–response relationship, which means that a stability criterion does not exist for launch vehicle aeroelastic coupling. The phasing between the force and response required for self-sustained oscillations can be explained in terms of the work conducted during the flow state changes.

References

[1]Chevalier, H. L., and Robertson, J. E., "Pressure Fluctuations Resulting from an Alternating Flow Separation and Attachment at Transonic Speeds," Arnold Engineering Development Center, AEDC TDR-63-204, Tullahoma, TN, Nov. 1963.

[2]Robertson, J. E., and Chevalier, H. L., "Characteristics of Steady-State Pressures on the Cylindrical Portion of Cone-Cylinder Bodies at Transonic Speeds," Arnold Engineering Development Center, AEDC TDR-63-104, Tullahoma, TN, Aug. 1963.

[3]Rainey, A. G., "Progress on the Launch-Vehicle Buffeting Problem," *Journal of Spacecraft and Rockets*, Vol. 2, No. 3, 1965, pp. 289–299.

[4]Fleming, E. R., "Transonic Buffeting Loads Experience at The Aerospace Corporation," Aerospace Corp., TOR-95(5530)-6, El Segundo, CA, March 1995.

[5]Ericsson, L. E., "Aeroelastic Instability Caused by Slender Payloads," *Journal of Spacecraft and Rockets*, Vol. 4, No. 1, 1967, pp. 65–73.

[6]Azevedo, J. L. F., "Aeroelastic Analysis of Launch Vehicles in Transonic Flight," *Journal of Spacecraft and Rockets*, Vol. 26, No. 1, 1989, pp. 14–23.

[7]Dowell, E. H. (ed.), *A Modern Course in Aeroelasticity*, 3rd ed., Kluwer Academic, Boston, 1995, pp. 472–532.

[8]Ericsson, L. E., and Reding, J. P., "Fluid Dynamics of Unsteady Separated Flow, Part I, Bodies of Revolution," *Progress in Aerospace Sciences*, Vol. 23, 1986, pp. 1–84.

[9]Fleming, E. R., "Launch Vehicle Loads," *Flight-Vehicle Materials, Structures, and Dynamics—Assessment and Future Directions, Vol. 1—New and Projected Aeronautical and Space Systems, Design Concepts, and Loads*, Sec. 2, A95-24426, American Society of Mechanical Engineers, New York, 1994, pp. 530–541.

[10]Macheske, V. M., Womack, J. M., and Binkley, J. F., "A Statistical Technique for Combining Launch Vehicle Atmospheric Flight Loads," AIAA Paper 93-0755, Jan. 1993.

[11]Dotson, K. W., and Tiwari, S. B., "Formulation and Analysis of Launch Vehicle Maneuvering Loads," *Journal of Spacecraft and Rockets*, Vol. 33, No. 6, 1996, pp. 815–821.

[12]Mango, F. S., "Recommendations of the Max Airloads High Performance Work Team," Martin Marietta Corp., IDC 3221-FE-T4/94-126, Denver, CO, Nov. 1994.

[13]Hart, P. M., and Schwerin, W. D., "Titan/Centaur Wind Tunnel Test Report," Martin Marietta Corp., MCR-71-276, Denver, CO, Sept. 1971.

[14]Crandall, S. H., *Engineering Analysis: A Survey of Numerical Procedures*, 1st ed., McGraw–Hill, New York, 1956, pp. 147–154.

[15]Dotson, K. W., Veletsos, A. S., and Ventura, C. E., "Dynamic Response of Simple Linear Systems to Periodic Forces," *Structural Research at Rice*, No. 26, Dept. of Civil Engineering, Rice Univ., Houston, TX, 1983.

[16]Craig, R. R., *Structural Dynamics: An Introduction to Computer Methods*, 1st ed., Wiley, New York, 1981, pp. 139–146, 163–169.

[17]Dotson, K. W., Baker, R. L., and Bywater, R. J., "Launch Vehicle Self-Sustained Oscillation from Aeroelastic Coupling Part 2: Analysis," *Journal of Spacecraft and Rockets*, Vol. 35, No. 3, 1998, pp. 374–379.

[18]Minorsky, N., *Nonlinear Oscillations*, 1st ed., Krieger, Malabar, FL, 1962, pp. 71–77.

[19]Reding, J. P., and Ericsson, L. E., "Hammerhead and Nose-Cylinder-Flare Aeroelastic Stability Revisited," *Journal of Spacecraft and Rockets*, Vol. 32, No. 1, 1995, pp. 55–59.

[20]Deniz, S., and Staubli, T., "Oscillating Rectangular and Octagonal Profiles: Interaction of Leading- and Trailing-Edge Vortex Formation," *Journal of Fluids and Structures*, Vol. 11, No. 1, 1997, pp. 3–31.

R. B. Malla
Associate Editor